# THERMAL-HYDRAULIC INVESTIGATIONS OF A HORIZONTAL ROD BUNDLE TARGET AT HIGH-POWERS DURING OPERATION

R. Milenković<sup>1</sup> and S. Dementjevs<sup>1</sup>

<sup>1</sup> Paul Scherrer Institut, Villigen PSI, Switzerland rade.milenkovic@psi.ch, sergejs.dementjevs@psi.ch

#### **Abstract**

In order to understand the complex hydraulic, thermal and structural behavior of the rod-bundle target of the Swiss Spallation Neutron Source-SINQ at PSI during operation at high powers, a well-controlled experiment has been conducted by increasing the proton beam current in stops, permitting steady state heat transfer conditions to be reached at different power levels. During the experiment, the total mass flow rate, the pressure loss in the target, temperatures at various locations, pressures at the inlet and outlet of the target and structural acceleration of the target head were acquired at various powers (i.e. steady-state conditions). Experimental data are used as benchmark boundary conditions for coupled thermal-structural analysis with the aim to evaluate and indentify reliable operating conditions.

#### 1. Introduction

The development of high-power spallation targets for neutron production has been conducted apace at PSI (Paul Scherrer Institut) driven by in-house and international projects, which demand increasing neutron production and keeping conservative safety measures. Spallation reactions take place when high-energy protons impact on a heavy target material made e.g. from lead, lead bismuth or mercury. Spallation neutron sources are part of in an innovative concept of generating energy, for sustaining a fission chain reaction in a subcritical reactor core (as in Accelerator Driven Systems-ADS).

Since the huge amount of heat deposited in the target and in the structural materials during spallation processes must be removed, the thermal-hydraulics simulations, studies, experiments and the associated structural analysis are constantly in the focus with the main objectives to indentify physical phenomena that affect cooling modes, to demonstrate reliable cooling and structural integrity and to indentify optimum design in order to minimize thermal loads and avoid hot spots.

#### 2. SINQ horizontal rod-bundle target

The current SINQ heavy water  $(D_2O)$ -cooled rod bundle target is schematically depicted in Figure 1. The target rod array is built from Zircaloy-2 tubes, which are filled with lead. The volumetric fraction of the lead inside the rods is about 90%, since it is necessary to allow for thermal expansion of the lead during heating up and melting.

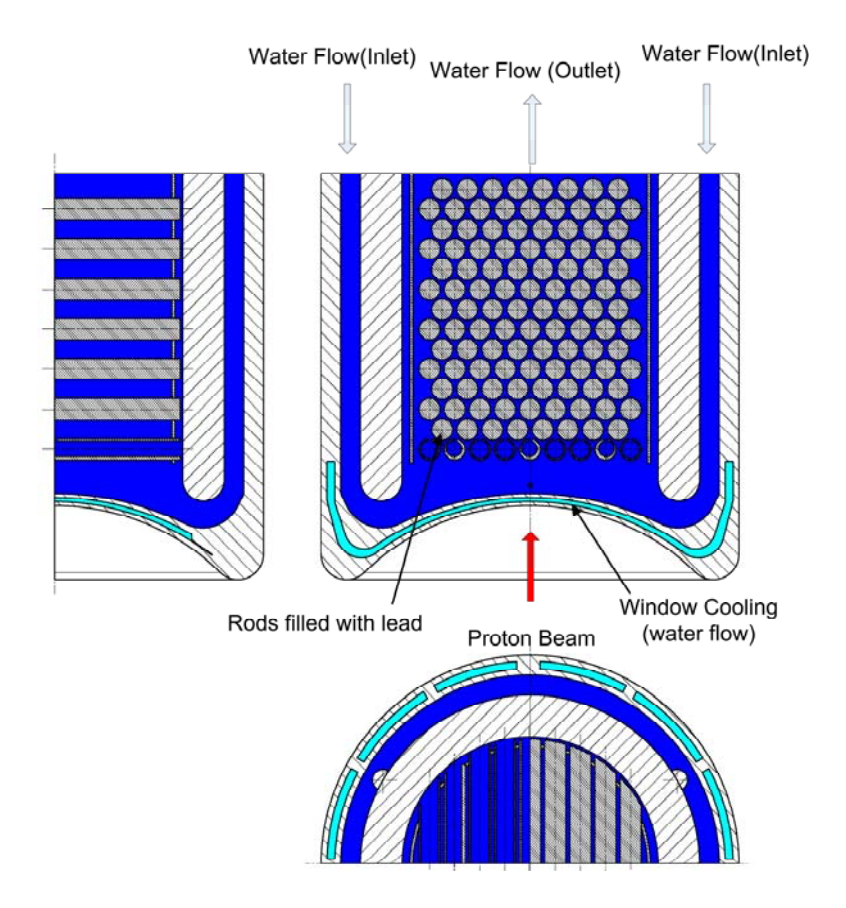


Figure 1 SINQ rod bundle target

The target configuration is vertical. The 575 MeV proton beam penetrates through the AlMg3 dome shaped Beam Entry Window (BEW) and hits the rod bundle from below. The target window reverses the water flow (D<sub>2</sub>O) (ca. 10 kg/s, 7 bar) coming down through the annulus and directs it through the main guide tube, where in the rod bundle is situated. The BEW is cooled by a separate water flow (2.5 kg/s), passing through the narrow channel between the two containment hulls. The heat deposition profile for the target structures has been calculated by using MC (Monte-Carlo) calculations with MCNPX 2.5.0 ([1]). The maximum power deposited into the target material (lead) reaches 480 W/cm<sup>3</sup> at a total beam current of 1.5 mA (current maximal value) and 640 W/cm<sup>3</sup> at a total beam current of 2.0 mA (planned to be achieved in the future after upgrading of the accelerator).

Depending on the flow conditions, the power and pressure in the system, several flow and heat transfer regimes may occur inside the target assembly. Apart from single phase convective heat transfer at the rod outer surface, nucleate boiling may occur in the wakes of the horizontal tubes. When vapor bubbles enter a region where the temperature drops, condensation may take place. Therefore, in some scenarios, the coolant flow can be also characterized as a complex two-phase flow.

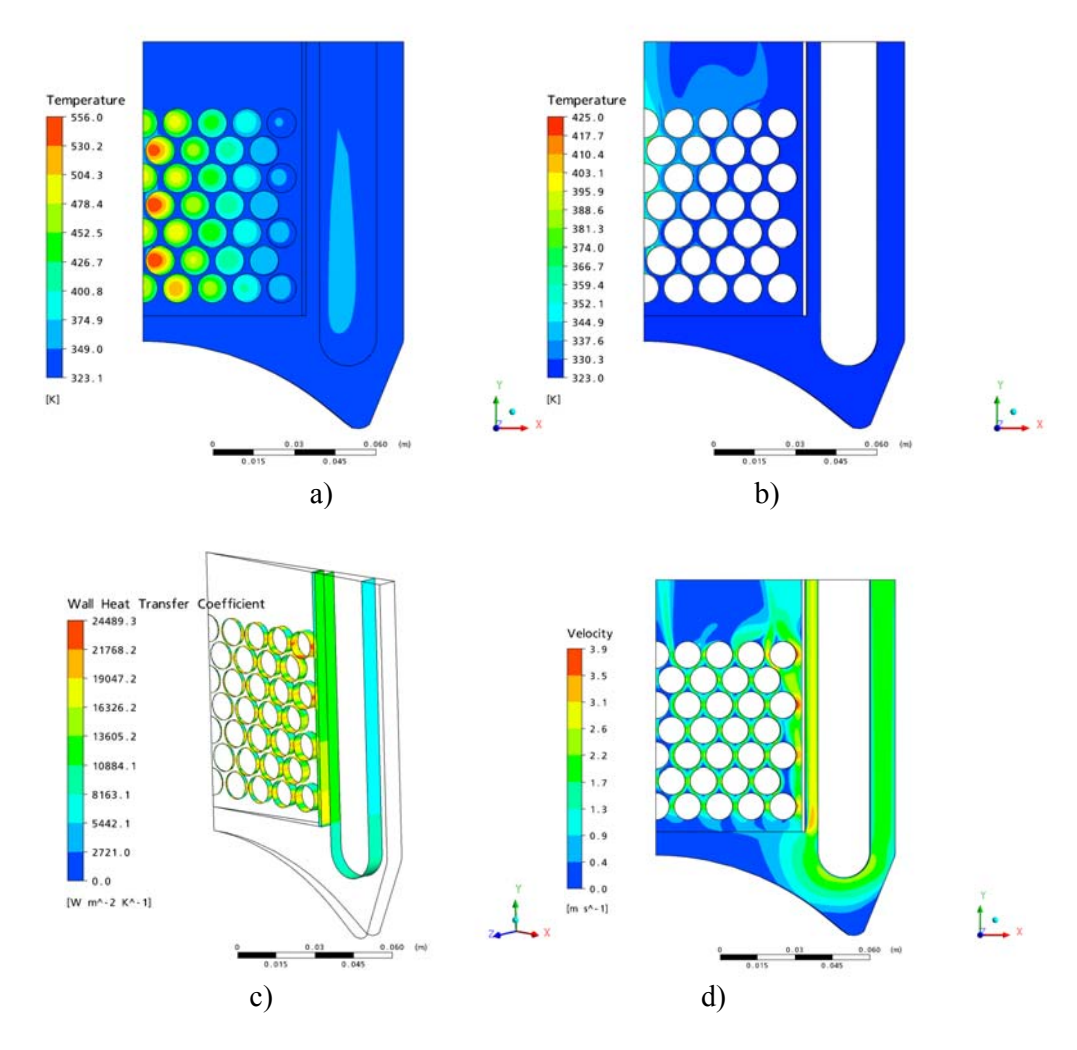


Figure 2 SINQ rod bundle target calculations with a simplified axisymmetric 2D model: a) temperature field, b) water (model fluid is H<sub>2</sub>O) temperature field (425 K is the boiling water temperature at 5 bar), c) wall heat transfer coefficient plot based on CFX calculations, d) velocity field. The results correspond to a peak power deposition of 480 W/cm<sup>3</sup>. The centreline rods, which are located at the model axis, are more strongly cooled because of the geometric modelling.

In order to examine the flow field at the inlet of the rod bundle for various operating conditions and to aid the design of current and future experiments, Computational Fluid Dynamics (CFD) is being used. Namely, a 2D model of the rod bundle target with the previously used window geometry comprised a fluid domain (Figure 2) with solid rods made of lead. The blanket was modeled as solid lead. Other structures were represented by adiabatic walls. A structured mesh with mesh enrichment near solid boundaries was used. Since the main computational task was to investigate the flow conditions at the inlet of the rod bundle, the model was parametric, where the number of rods and the corresponding mesh could be adjusted. In addition, a separate fluid (sub-) domain was added at the outlet in order to model additional flow resistances. In order to model these resistances a directional momentum loss model with a quadratic resistance coefficient is used in the defined subdomain. The quadratic resistance coefficient has been estimated based on total pressure loss

measurements [2] in a mock-up of the rod bundle. The computational results shown in Figure 2, which have been obtained for the thermal power with peak value of 480 W/cm³, indicate that surface temperatures may reach the boiling temperature of water at the pressure of 5 bar. Therefore, one can expect subcooled boiling for such high powers and for some flow regimes (see Figure 2d) mainly around the target centerline in the lower part of the target. Further downstream, rod surface temperatures are below the boiling point and existing bubbles condensate.

## 2.1 Main objectives

All thermal-hydraulic and structural studies have been unified in the project called <u>Cool</u>ability of the Rod-<u>Bundle Target</u> for SINQ (COOLBUNT). The objectives are:

- to examine the thermal-hydraulic behavior;
- to indentify special phenomena that affect cooling; and
- to establish conservative safety margins on target coolability.

As the second study of the project, an experiment has been launched in order to study effects of the various powers, i.e. beam currents, on the thermal-hydraulic behaviour of the SINQ target and to determine local single-phase heat transfer coefficients for rods in a bundle during operation.

# 2.2 Brief explanation of the SINQ control system

As the current control system is based on regulation of the pressure at the inlet of the target, the pressure of Helium in the expansion tank and, therefore, the pressure at the outlet of the target rise during operation at high powers (since the temperature increases). This change affects the total pressure loss and, of course, the total mass flow rate through the target. Therefore, one may expect that the mass flow rate will drop during operation of the target when the power is gradually increased. As it is usually desirable to have constant mass flow rate, this is the main disadvantage for conducting steady-state heat transfer tests at high powers during operation. This issue affects the choice of methods to be used for detection of local boiling phenomena.

## 3. Experimental results

# 3.1 Experimental procedure

This well-controlled experiment was conducted by increasing the proton beam current by steps and permitting after steady-state heat transfer conditions to be reached at each power level. At each power level, the beam current was kept constant during 15 min. Due to the unpredictable behavior of some accelerator components; several beam trips occured during the test. The total mass flow rate, the pressure loss in the target, temperatures at various locations, pressures at the inlet and outlet of the target and structural acceleration of the target head were acquired at various powers (i.e. steady-state conditions).

#### 3.2 Instrumentation

Figure 3 shows where the acceleration sensors were installed on the target head, and Figure 4 gives a layout of the thermocouple positions inside rods built from Zr-2 in rows 9 and 34. As the structural acceleration data carry information on coupled fluid-structure interactions, the main objective was to detect indirectly any kind of abnormal system behaviour during operation at normal and enhanced powers. The sensors were installed on the target head; clearly a location where piezo-crystals can survive during operation, but far way from an optimal position where one could expect high signal-to-noise ratio.

As the signal generated by the acceleration sensor at this location is very small, the method may be also sensitive to electromagnetic interference. Since the sensor cables could not be isolated from the electrical power lines, the power line-harmonics were expected to be clearly seen in the full frequency domain. Anyway, based on experience gained during some liquid metal tests (see [3]), the signal was regularly acquired every hour at 20 kHz during several minutes for several months. The results are presented in Chapter 3.6.

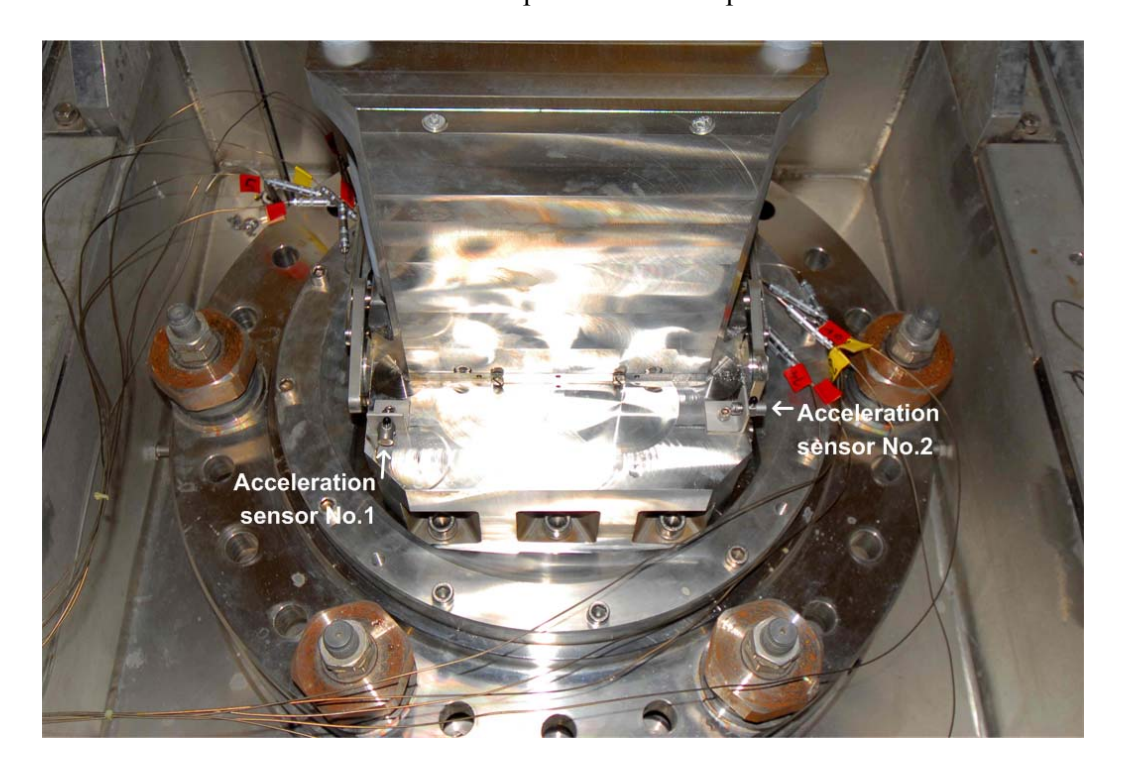


Figure 3 Structural acceleration sensors installed during shut down at the target head.

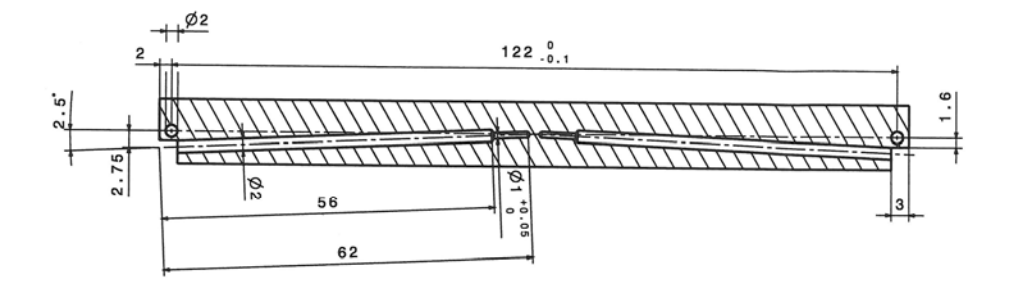


Figure 4 Thermocouples installed at the centerline rods in rows 9 and 34.

In order to monitor the thermal behavior of the target and to provide data for computational studies, thermocouples (type K) were installed in the centerline rod in rows 9 and 34. The thermocouples located in row 34 worked correctly until the end of life of the target, whereas those located in row 9 failed after approximately a year of operation. Both centerline rods have been made of Zircaloy-2. Even though all four thermocouples have been installed using the same method, no guarantee could be provided regarding the thermal contact between the rod and tip ends. The results are presented in the Chapter 4.

## 3.3 Beam current data (i.e. thermal power)

The experiment was conducted by varying the beam current in steps (each of them 0.2 mA) from zero to maximum power that corresponds to 2.2 mA (see trend lines in Figure 5). The beam line before the SINQ target is equipped with plenty of beam current monitoring points; several relevant trends are shown here. The experimental data collected during our experiment are basically saved into two different databases, which are not synchronized, but the beam current is the joint parameter. Therefore, the only possibility to compare and correlate operational and vibration data acquired at several order of magnitude different sampling rates, was to perform cross-checking of the time stamps related with the beam current variable.

The closest measurement point (marked as MHC 5 in Figure 5) is located ca. 6.5 m away from the target. There are no monitoring points just in front of the target. Approximately, the maximum current of 2.2 mA at MHC 4 corresponds to 1.5 mA at MHC 5 (ratio of approximately 2/3), because another target, called target E, is placed and operated in the same beam line. The peak thermal power density in W/cm³ for the Zircaloy-rod in row 9 for each beam current value at the SINQ monitoring point can be estimated by multiplying the beam current in μA with the factor of 0.32 [1]. This constant for the Zircaloy-rod in row 34 is 0.102, which means that here the peak power is 3 times lower. The beam trips, which can be easily spotted in Figure 5, occur regularly during normal operation. The MHC 5 trends recorded in the AC and SINQ database do not match. This fact highlights imperfections of the system used for saving the SINQ operational data. Basically, the increased time offset at high powers between two trends and disagreeing values in the SINQ line trend indicated some problems with data transfer and saving. Nevertheless, this issue is irrelevant for steady state analysis, since all operational data including beam current values are taken during stable steady states.

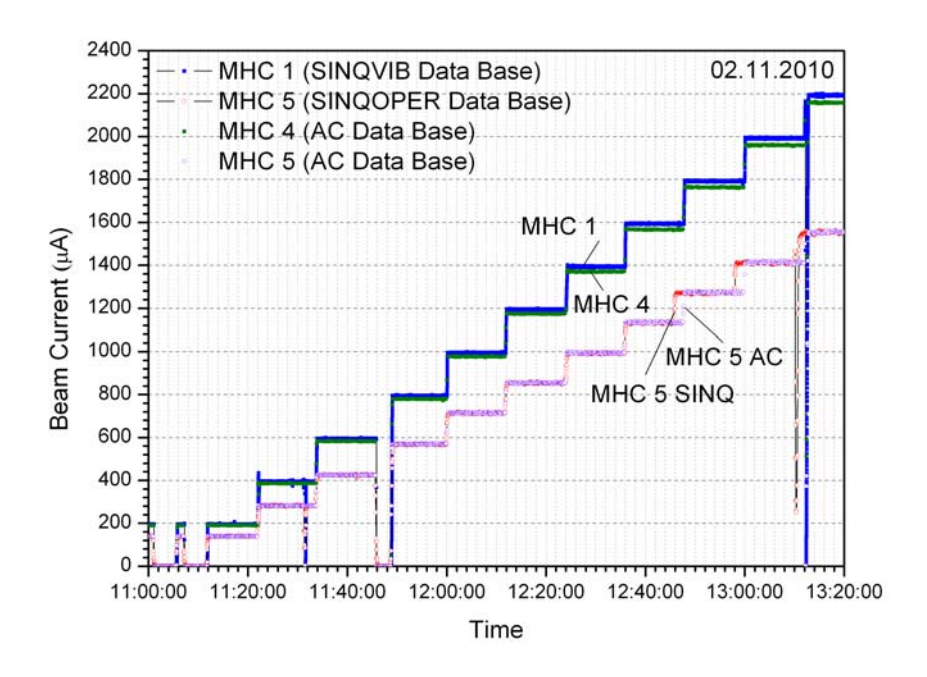


Figure 5 The experiment was conducted by varying the beam current in steps (each of them 0.2 mA) from zero to maximum power. The beam current data have been monitored at several locations along the beam line. The closest monitoring point to the SINQ target is presented as MHC 5. These data are saved into the SINQ database, whereas data taken further way from the target are saved into another database.

### 3.4 Operational flow parameters

What does a target make to be a unique and interesting system for thermal-hydraulic and structural examinations? The large amount of heat deposited into a small volume may locally create an overheating of exposed target structural parts, in this case rods filled with lead. Accompanied thermal stresses can lead to structural failure and shutting down of the system. To analyse the possibility of having increasingly powerful proton beams, two ways for examining the thermal-hydraulic and structural behaviour of a high-power spallation source are employed during this study: an experimental investigation and numerical simulations with up-to-date codes. An overview look of such an experiment with some zoomed details is summarized in Figures 6 and 7. Namely, the total mass flow rate, the pressure loss in the target, the pressure at the inlet and outlet of the target at various power levels visualize how the current control system works and prove that detection of local phenomena such as nucleate boiling, condensation, transition between single-phase, bubbly or slug flows is practically impossible. The detected long-time decreasing trend of the pressure loss with increasing power arises because the pressure at the inlet is controlled and kept constant (it stabilizes at higher power-see Figure 7), the pressure at the outlet rises due to increasing pressure of the cover gas. The result is that the target at high temperature and power operates at slightly lower flow rate than at low powers.

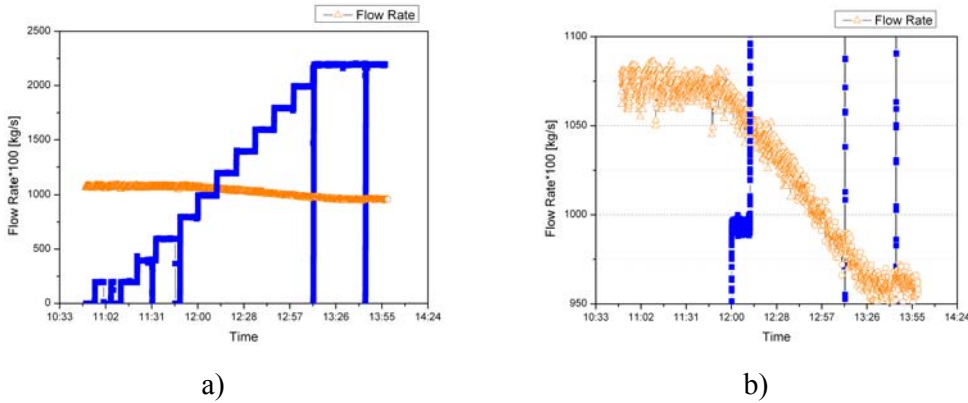


Figure 6 Flow rate and power level vs. time: a) full trend; b) zoomed flow rate drop. The steady state condition, which is captured on the right at about 12:00h, corresponds to the beam current of  $800\mu A$ .

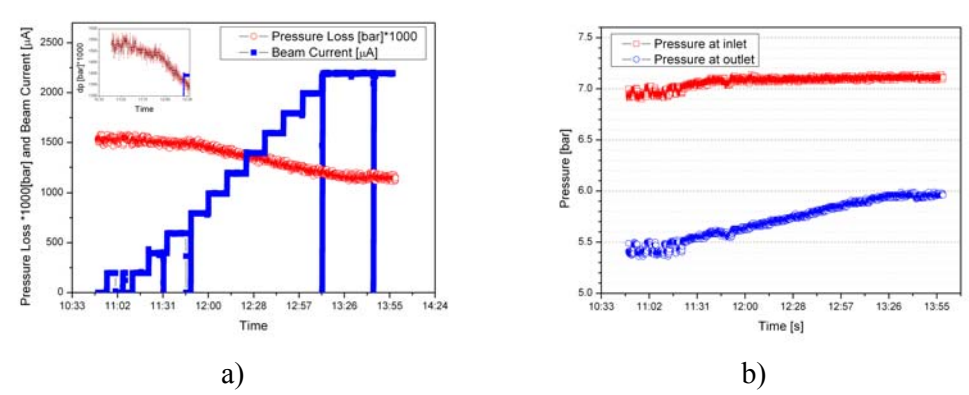


Figure 7 Pressure measurements during the experiment: a) pressure loss; b) pressure at the inlet and outlet of the target.

## 3.5 CFD simulations and comparisons with experimental results

A CFD analysis (heat conduction in the rod, constant heat transfer coefficient at the outer surface and constant bulk fluid temperature, see Figure 9) of a Zircaloy rod equipped with two thermocouples for a constant power density of 480 W/cm³ showed good agreement between calculated and experimental data (see Figure 9 a). The imposed boundary conditions were: a constant heat transfer coefficient and the water bulk temperature. In order to estimate the water bulk temperature in row 34, experimental results presented in Figure 9d were taken into consideration. They show that the water bulk temperature at the rod bundle inlet increases with power increase. If we take a value of approximately 50°C obtained from thermocoupleses CT010 and CT011 at row 9, the bulk water temperature at row 34 can be calculated from the thermal balance assuming the total exchanged power of 600 kW. The water flow rate is 9.5 kg/s. The calculated value is about 64 °C at row 34. A good agreement with experimental data (Figure 9a) is achieved with the heat transfer coefficient of 27000 W/m²/K and the bulk water temperature of 64°C.

The highest local surface temperature calculated with the same model for a rod in row 9 is about 103 °C and it is below the boiling temperature at 5.5 bar (155.34°C, H<sub>2</sub>O). Unfortunately, since both thermocouples installed in the rod in row 9 failed after

approximately a year of operation, the experiment described here could be conducted only with thermocouples installed further downstream in row 34.

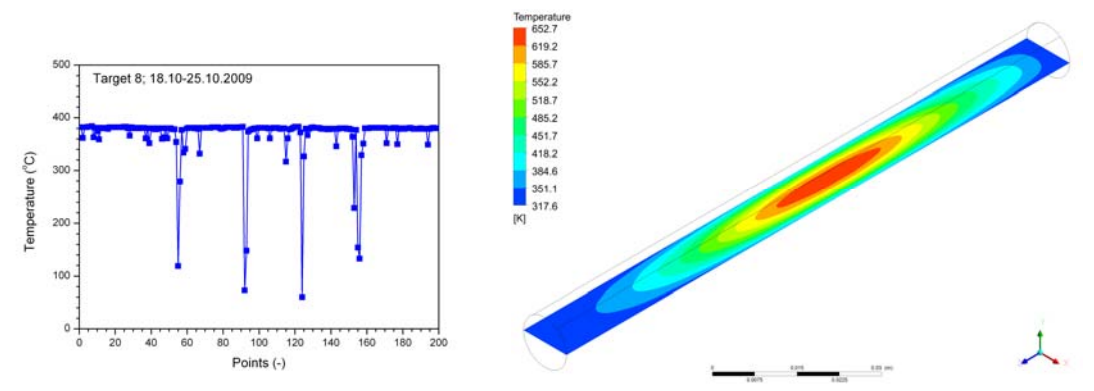


Figure 8 Temperature measurements obtained earlier by the thermocouples installed in the rod in row 9 (left) and the temperature field inside the rod calculated for mentioned boundary condition (right).

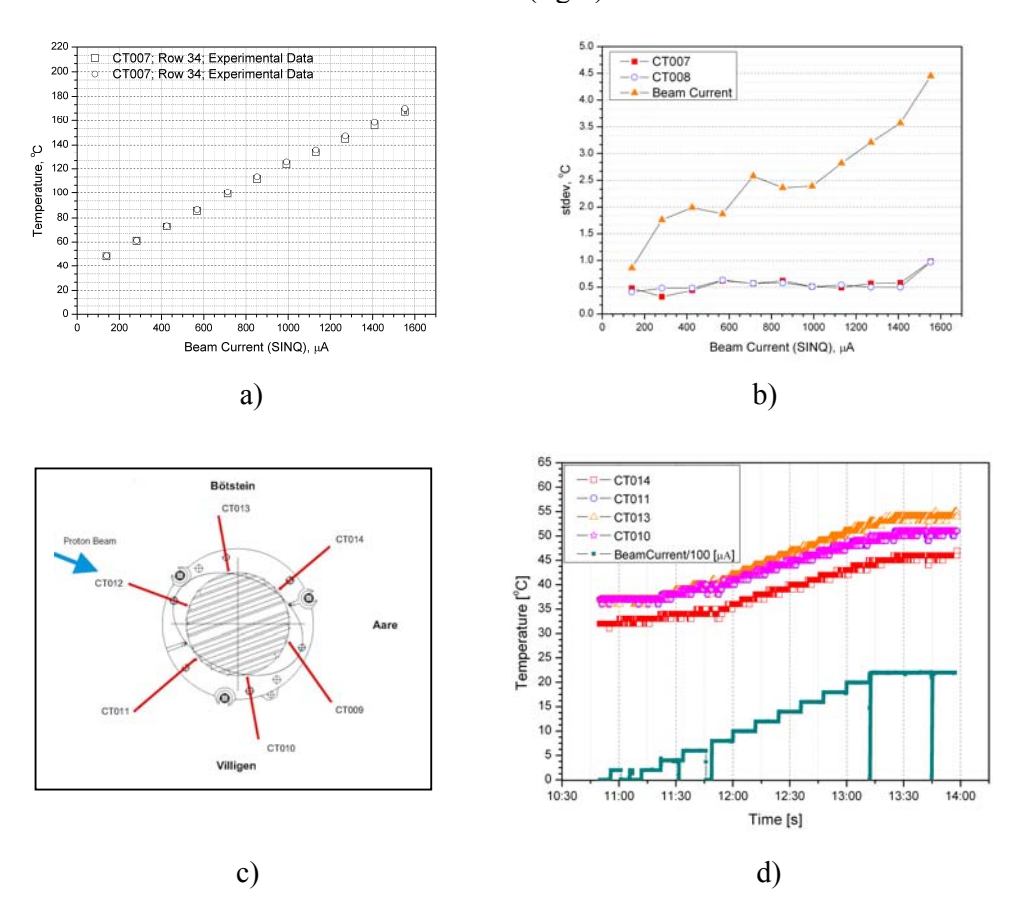
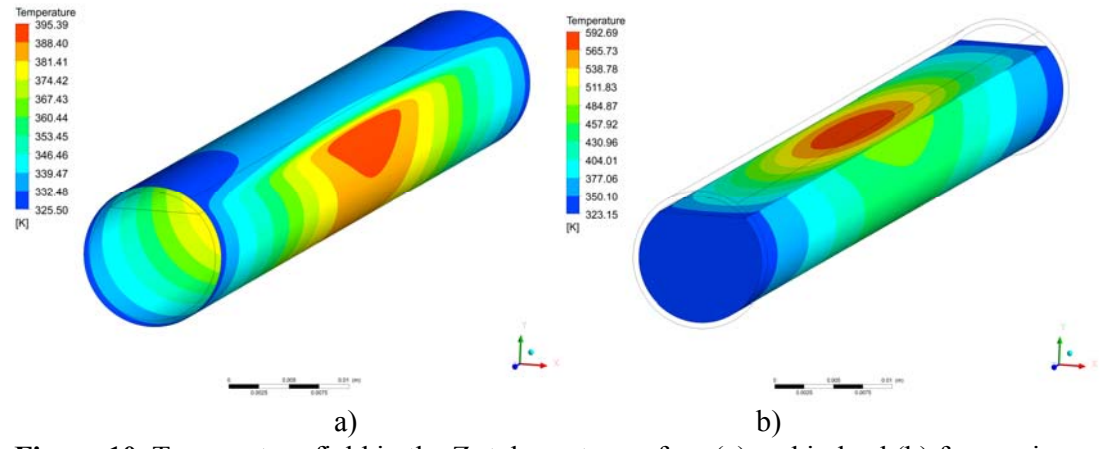


Figure 9 Comparison between computational and experimental results (a) and standard deviation of temperature measurements (b) indicate a possible heat transfer regime change. Beam trips are excluded for the calculation of the statistical parameters; c) locations of the thermocouples at the inlet of the rod-bundle target; d) water temperature measurements at the inlet of the rod bundle at different powers.

Flow rate and pressure loss data are given in Figure 7. It is clearly shown that the flow rate drops at high powers due to the change of the pressure at the outlet. Also, from the plot shown in Figure 9d, the temperature variance at beam current of 1550µA is 100% higher than at the beam current from 0 to 1550µA. Beam trips are excluded from the analysis. At this power we performed only one steady-state measurement. In addition, it must be mentioned that the thermocouples installed in row 9, where for the same beam current 3 times higher power is deposited, had failed. If subcooled local nucleate boiling would have occurred in the bottom region of the target, where the peak power is located, would it be possible to detect a change of the heat transfer regimes downstream due to possible vapor condensation since the temperature at the surface of the rod bundle drops below the boiling temperature and the bulk fluid temperature is even lower? Such complex behavior may affect temperatures measured with thermocouples in row 34, even though the thermocouples are installed inside the rod. Additional experiments with a new configuration are to be conducted in the near future.



**Figure 10.** Temperature field in the Zr tube-outer surface (a) and in lead (b) for maximum power deposited (peak power of 480 W/cm<sup>3</sup>) and the same boundary conditions as for Zr-rod (the heat transfer coefficient of 27000 W/m<sup>2</sup>/K, the bulk water temperature of 55°C).

Figure 10 shows the computational results obtained with a model of a Zr-2 tube filled with lead for peak power of 480 W/cm<sup>3</sup>. The thermal contact between lead and Zircaloy is modeled as the perfect one. The heat transfer in the gap between the free lead surface and inner rod surface is modeled as a convective one with low heat transfer coefficient (ca. 5 W/m<sup>2</sup>/K). The bulk temperature of 55 °C is calculated based on the thermal balance at row 9 for given inlet water temperature of 50 °C. The temperature distribution indicates that the lead temperature approaches the melting point and the surface temperature is close to the water boiling temperature at 5 bar.

#### 3.6 Structural vibrations under real operational conditions

In order to check the vibration characteristics of the target and to detect impacts, all experimental data have been analyzed by advanced time-frequency methods such as Short-Time Fourier Transform (STFT). As various phenomena and instabilities, such as flow

turbulence, vortex shedding, large coherent structures, nucleate boiling and condensation generate forces, they affect directly structural acceleration and displacement. Obviously, if vibration (or similar) structural measurements had been possible in the vicinity of the region where the proton power is deposited, the results would have been easier to interpret and maybe would have brought more information simply because the signal-to-noise ratio would be higher. In our case the ultimate location, where these sensors could have been installed, was on the target head. In order to distinguish between various possible sources of instabilities, the experiments were systematically conducted for no power and for various steady-state conditions (the power was changed in steps). For the first time, an attempt was made to determine characteristic vibration patterns connected with the structural behavior of the target head at various powers.

The raw signals taken with acceleration sensors shown in Figure 3, contain high power contributions from the power-line harmonics, as it can be clearly seen in Figure 11 b. The amplitude and power of each harmonic may significantly vary from one record to another (not shown here). Under these conditions any irregularities caused by flow-induced vibrations could not have been systematically studied, because the signal power in the frequency domain was too low. The power of background noise could have been removed by setting-up a threshold of the Gabor coefficients (Short-time Fourier Transform with Gaussian Window). Notch filters have also been tested, but without success. In addition, if any of the characteristic system frequencies would have coincided with those of the power-line, it would not have been possible to distinguish and to detect the real source of instability. Anyway, in order to provide information for engineers and researchers who are involved in structural measurements for diagnostic purposes, the following characteristic findings are shown in Figures 11 and 12.

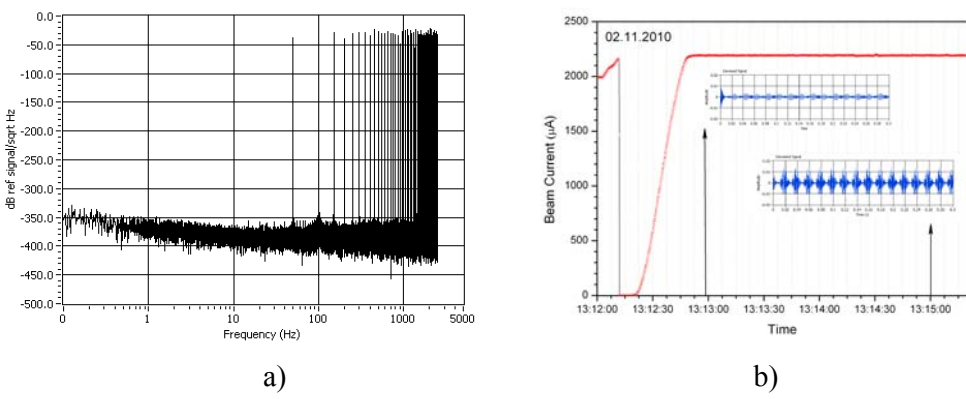


Figure 11 Spectrum of power-line harmonics at 0.0 mA (a) and beam trip with denoised signal (b).

Figure 11a shows a typical beam trip and denoised response signal from an acceleration sensor at the times marked with arrows. It is clear that acceleration sensors do not respond immediately to the beam trip, but a significant difference in power and frequency domain (not shown here) is observed. Power-line harmonics are present in both signals.

In August 2010 two characteristic amplitude peaks (called here impacts) were detected (see Figure 12).

High power values of power-line harmonics (in the power spectrum) have been captured in the data in July (before the impacts) and in August (after the impacts illustrated in Figure 12). While in July high power is not present all the time (these events occur randomly in the full frequency range), in August some strong harmonics could be detected in the full data set all the time. In May and June nothing happened (before the impacts). Anyway due to the existence of strong power-line harmonics, it is impossible to distinguish resonance frequencies. Based on experience gained during our structural tests done with a prototype of the EURISOL target [4], where we detected the resonance frequencies, the vanes and spot welds (see the design of the target in [5]) were ruptured and we detected strong final impacts. The experiment described in [3] was shut down without problems.

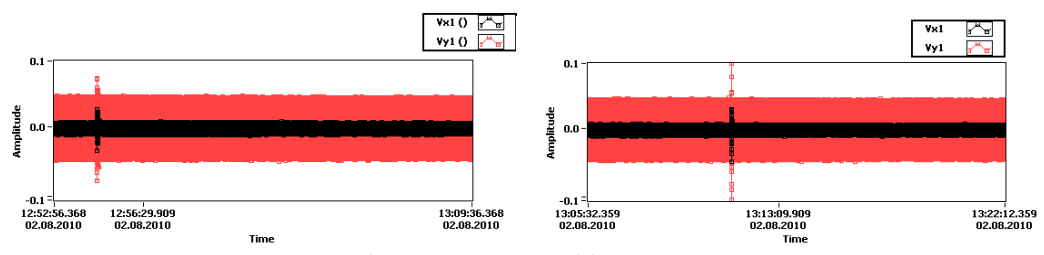


Figure 12 Detected impacts

During SINQ vibration monitoring we detected two structural impacts. Independently, high activity detected in  $D_2O$  proved that the some structural components in the target may have failed. More details on the nature of the failure will be available in the future.

# 4. Conclusion

The thermal-hydraulic and structural behaviour of the SINQ target was examined during operation at low, intermediate and high powers. The target cannot be easily instrumented because of various restrictions. Basically, due to restricted space for cables, several sensors and thermocouples can only be installed before the target is irradiated. Since some sensors failed during 2 years operation, planned and carefully conducted experimental investigations at the initial state of operation or after shut-down during beam start-up are of high practical and scientific importance. The results of our tests showed the following:

- As it is not possible to install instruments at the most relevant locations in the target, meaningful results can only be obtained by combining various methods such as CFD, thermal-hydraulic analysis of reference conditions and online operational experiments. We performed such a coupled analysis for a rod made of Zr-2 in order to define boundary conditions for examining the structural behaviour of more complex units such as rods filled with lead.
- Even though the structural measurements were conducted on the target head, far away from the region of interest, differences of system behaviour were observed during operations at different powers. Due to the existence of strong power-line harmonics, it was however impossible to identify any structural resonance frequencies. Anyway, two structural impacts could be detected, as shown in Fig. 12, and the powers of some power-line harmonics were irregularly increased before the impacts happened. The fact that the some structural components failed, i.e. a contamination was detected in the D<sub>2</sub>O loop, proved that it may be possible to use remote monitoring techniques such as accelerometers to monitor the integrity of a target, including internal

components, which are not accessible by standard measurement techniques because of geometrical and material constraints. The illustrated capability of vibration measurements could improve safeguard and operational procedures for high-power components in the radioactive environment on nuclear facilities.

## Acknowledgment

The authors are grateful to Davide Reggiani for his valuable assistance for proton beam operation during the experiment and Michael Wohlmuther for his Monte Carlo calculations of heat deposition profiles. Valuable contributions to the test set-up, in particular to the data acquisition, by Enzo Manfrin are gratefully acknowledged. The authors are thankful to Frank Heinrich and Mike Seidel for fruitful discussions, advice and support.

#### 5. References

- [1] Wohlmuther, M., "Energy Deposition Calculations", private communication, 2010.
- [2] Müller C., "Thermohydraulische Optimierung des SINQ Targets", 2007.
- [3] R. Milenković, S. Dementjevs, K. Samec, E. Platacis, A. Zik, A. Flerov, K. Thomsen "Structural-hydraulic liquid metal test of the EURISOL target mock-up", Nuclear Instruments and Methods in Physics Research Section A, Vol. 607, Issue 2, 2009, pp. 279-292.
- [4] R. Milenković, K. Samec, S. Dementjevs, A. Flerov, W. Wagner, "Detection of a structural impact in liquid metal flow during test runs of the EURISOL target mock-up" Nuclear Instruments and Methods in Physics Research Section A, Vol. 609, 2009, pp. 1-18.
- [5] K. Samec, R. Milenković, S. Demetjevs, M. Ashrafi-Nik, A. Kalt, "Design of a compact high power neutron source", Nuclear Instruments and Methods in Physics Research Section A, Vol. 606, Issue 3, 2009, pp. 281-290.